EUROPEAN LABORATORY FOR PARTICLE PHYSICS

CERN SL DIVISION

CERN-SL-95-64 OP

Centre-of-Mass Energy Shifts from Difference Dispersion and Collisions Offsets in Pretzel Operation at LEP

J. Wenninger

Abstract

At the interaction points of LEP dispersion induces correlations between the energies and transverse positions of the particles and influences the centre-of-mass system energy distribution. Unequal dispersion of the beams leads to a reduction of the energy spread. Additional transverse collision offsets cause shifts of the average centre-of-mass energy. Such modifications of the energy distributions have not been taken into account up to now for the LEP energy calibration. This report summarizes an analysis of collision offsets and difference dispersion at the interaction points for the 1993 and 1994 Pretzel operation runs of LEP. The resulting systematic error on the centre-of-mass energy is estimated to be 0.4 MeV for the 1993 LEP energy scan and 0.7 MeV for the 1994 LEP run. The reduction of the centre-of-mass energy spread does not exceed 0.2%.

Geneva, Switzerland

12 June 1995

Contents

1 Introduction

In the past five years of LEP operation around the Z resonance, the understanding of the beam energy has been greatly improved with the help of frequent and accurate calibrations by resonant depolarization [1]. Following the 1993 energy scan the contribution to the Z mass and width errors from the calibration of the beam energy was reduced to about ± 1.5 MeV [2]. To achieve this result local energy corrections due to the energy sawtooth and the RF system, that cannot be measured by resonant depolarization, had also to be understood with high accuracy.

Following a successful test in 1994 [3], LEP is presently operated with bunch trains and not with the Pretzel scheme used in 1993 and 1994. A particular feature of this new scheme is the presence of significant amounts of vertical dispersion at the interaction points (IPs) [4]. This vertical dispersion, of opposite sign for both beams, is generated by the vertical electrostatic bumps required to avoid collisions at the parasitic beam encounters. A correction to the centre-of-mass (CM) energy at the IPs related to dispersion differences in combination with collision offsets has been identified recently in a study triggered by some side effects of the bunch train scheme [5]. Like the RF system corrections these potentially large CM energy shifts ($\sim$ MeV) cannot be measured directly. This effect, which is particularly important for bunch train operation and which introduces additional complications for a possible energy scan in 1995, had not been considered in the evaluation of the errors for the 1993 energy scan [2].

In this report I will first briefly summarize the problem due to dispersion and collision offsets at the IPs. Most of this document is then devoted to an analysis of these quantities for the

1993 energy scan and for the 1994 LEP run. I will conclude with an estimate of the importance of the CM energy shifts for the 1993 and 1994 LEP runs.

2 Effects of Dispersion at the Interaction Points

In a storage ring the dispersion $D(s)$ is a periodic function of the path length s which describes the behavior of off-momentum particles. Particles with an energy deviation δE from the nominal energy E follow a closed orbit $u_\delta(s)$ given by

$$u_\delta(s) = u_c(s) + D(s)\frac{\delta E}{E} \tag{1}$$

where u_c is the closed orbit of particles with nominal energy. The coordinate u can be either horizontal (x) or vertical (y). A non-zero dispersion introduces a correlation between the transverse position and the energy of the circulating particles. In the horizontal plane of LEP the average arc dispersion of about 75 cm is made to vanish in the straight sections with the help of dispersion suppressors. For a perfectly flat vertical orbit there is no vertical dispersion, but in the real machine imperfections and vertical bumps (magnetic and electrostatic) create a few centimeters of vertical dispersion. The vertical dispersion must be kept as small as possible since it can lead to performance degradation through an increase of the vertical beam emittance and of the beam sizes at the IPs.

If the dispersion of the e^+ and e^- beams differ at the IP in plane u, the correlation between transverse position and energy can lead to CM energy shifts ΔE_{CM} at the IP :

$$\Delta E_{CM} = -\Delta u^* \, \frac{\sigma_E^2 \, (D^*_{u1} - D^*_{u2})}{E \, ({\sigma^*_{bu1}}^2 + {\sigma^*_{bu2}}^2)} \tag{2}$$

where Δu^* is the collision offset between the two beams. σ^*_{bu} and D^*_u are respectively the total beam size and the dispersion at the IP. σ_E is the beam energy spread and E is the beam energy. The two beams are labeled by (1) and (2). ΔE_{CM} does not not vanish as soon as $\Delta u^* \neq 0$ and $D^*_{u1} \neq D^*_{u2}$. At the same time the CM energy spread $\sigma_{E_{CM}}$ is reduced, especially when $D^*_{u1} = -D^*_{u2}$ which is ideally the case for dispersion created by electrostatic bumps. $\sigma_{E_{CM}}$ is then no longer given by the simple incoherent addition of the energy spread of the beams :

$$\sigma^2_{E_{CM}} = 2\sigma_E^2 \, \kappa \tag{3}$$

$$0 \,\leq\, \kappa = \frac{1}{2}\left[\frac{(\sigma_E/E)^2 \, (D^*_{u1} + D^*_{u2})^2 + 4{\sigma^*_u}^2}{{\sigma^*_{bu1}}^2 + {\sigma^*_{bu2}}^2}\right] \,\leq\, 1 \tag{4}$$

σ^*_u is the beam size at the IP in absence of dispersion. It depends on the betatron function at the IP β^*_u and on the beam emittance ε_u and it is related to σ^*_{bui} through

$${\sigma^*_{bui}}^2 = {\sigma^*_u}^2 + \left(\frac{\sigma_E D^*_{ui}}{E}\right)^2 = \beta^*_u \varepsilon_u + \left(\frac{\sigma_E D^*_{ui}}{E}\right)^2 \tag{5}$$

More details can be found in [5, 6]. This *monochromator effect* is particularly important for bunch trains in the vertical plane where the beam sizes are small and significant differences in dispersion are expected. Because the horizontal beam size at the IP is rather large ($> 200\ \mu$m), the CM shifts are very small in that plane. The monochromator effect has not been taken into account for the analysis of the 1993 energy scan. In the case of Pretzel operation the difference dispersion generated by imperfections and electrostatic separators is expected to be small at the IPs. Never the less the error arising from this effect may not be entirely negligible a priori in comparison to the quoted error of ± 1.5 MeV of the Z mass and width.

3 Collision Offsets and Crossing Angles

The particles stored in LEP oscillate around the equilibrium closed orbit. The closed orbit $u_c(s)$ is a periodic function of the path length s which depends on all dipole deflections θ_i encountered on the ideal orbit along the ring [7] :

$$u_c(s) = \frac{\sqrt{\beta(s)}}{2\sin(\pi Q)} \sum_i \sqrt{\beta_i}\theta_i \cos(|\mu(s) - \mu_i| - \pi Q) \tag{6}$$

β and μ are the local betatron function and phase advance. Q is the machine tune for plane u. In the region between two consecutive deflections the closed orbit follows a betatron oscillation whose amplitude is modulated by $\sqrt{\beta(s)}$ as a function of the phase $\mu(s)$. For the difference closed orbit between the e^+ and e^- beams the effects of magnetic elements cancel and only electrostatic elements deflecting the beams in opposite directions have to be considered in Equation 6. Collision offsets and crossing angles of the beams at the IPs can be extrapolated from the difference of the e^+ and e^- closed orbits. In the absence of electrostatic elements the difference orbit in plane u follows a betatron oscillation :

$$\Delta u_c(s) = u_{c,e+}(s) - u_{c,e-}(s) = \sqrt{\beta(s)}\,[\,A\cos(\mu(s)) + B\sin(\mu(s))\,] \tag{7}$$

where A and B are oscillation amplitudes. This simple form is adequate to perform fits of difference orbits around the IPs. If the definition of the phase advance is such that $\mu = 0$ at a given IP, the beam separation (collision offset) at this IP Δu^* is given by

$$\Delta u^* = \sqrt{\beta^*}A \tag{8}$$

and the beam crossing angle at the IP θ_u^* by

$$\theta_u^* = \frac{B}{\sqrt{\beta^*}} \tag{9}$$

since $d\mu/ds = 1/\beta$ and $d\beta/ds = 0$ at the IP. β^* is the betatron function at the IP.

4 Analysis of Difference Orbits and Collision Offsets

The analysis of the collision offsets has been performed on a total sample of 1577 orbits. The 1993 data sample consists of 568 orbits, the 1994 data sample of 1009 orbits. The analysis covers 338 LEP fills. All orbits were acquired during physics conditions. For IPs 4 and 8 this analysis has not been carried out for the last period of November 1994. The vertical electrostatic bumps used to test the bunch train scheme would require a different approach for the analysis.

4.1 Fits of the Horizontal Difference Orbits

In 1993 and 1994 LEP has been running most of the time with Pretzel orbits. These orbits are produced with 8 electrostatic separators located next to the quadrupole QS11 on both sides of IPs 2, 4, 6 and 8 where the LEP experiments are installed. As a consequence the fits were only performed between pickups PU.QS10.L and PU.QS10.R because this area is free of horizontal

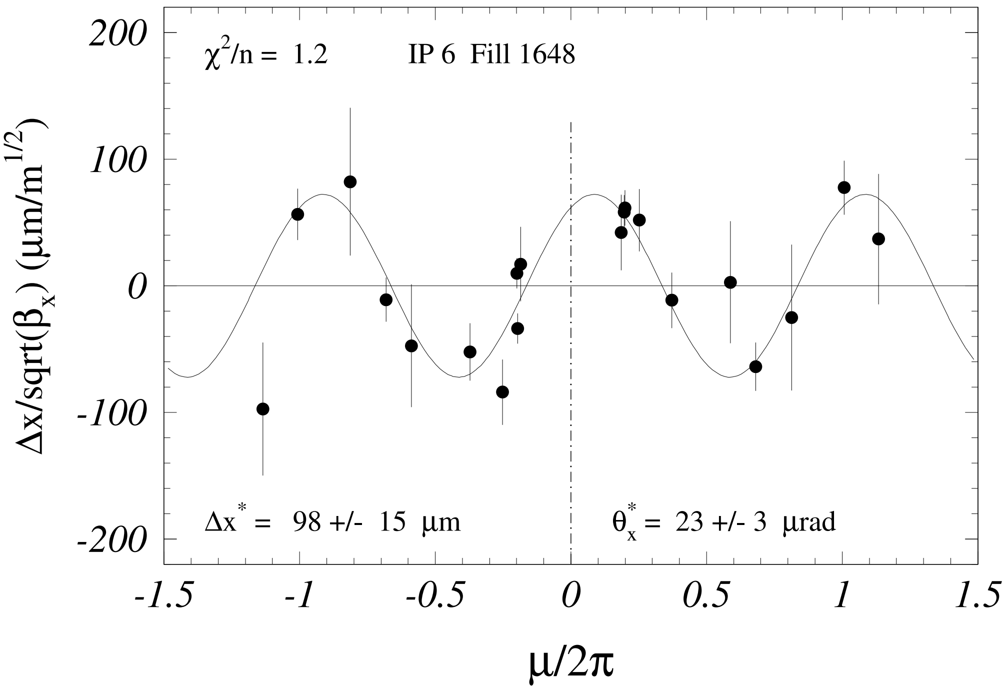

Figure 1: Example of the fit of a measured horizontal e^+e^- difference orbit between PU.QS10.L6 and PU.QS10.R6. The difference orbit normalized by the square root of β_x is shown as a function of the horizontal phase advance μ around IP6 which corresponds to $\mu = 0$. The fitted oscillation is superposed on the data points.

electrostatic elements. The measured difference orbit $\Delta x(s)$ is normalized by $\sqrt{\beta_x}$ and adjusted to a simple oscillation :

$$\frac{\Delta x(s)}{\sqrt{\beta_x(s)}} = A\cos(\mu(s)) + B\sin(\mu(s)) \qquad (10)$$

using phases and betatron functions calculated with the MAD program [8]. The horizontal betatron function at the IP is $\beta_x^* = 2.5$ m for 1993 and $\beta_x^* = 2.0$ m for 1994. In the region used for the fit β_x varies at the beam orbit monitor pickups between 10 and 300 m. An example of a fit is shown in Figure 1. The pickup measurement errors have been scaled to obtain an average χ^2 per degree of freedom of 1. The magnitude of the errors used for the fits ($\sim$ 150 μm) is in agreement with the systematic errors measured with the K-modulation technique for the different particle types and electronic gains [9]. The errors on the betatron functions due to beta-beating have been set to 20% for the 1993 data and to 10% for the 1994 data as indicated by the 1000-turn measurements [10]. The systematic errors on the collision offset and the crossing angle are estimated to be ± 15 μm and ± 10 μrad respectively.

4.2 Fits of the Vertical Difference Orbits

For the vertical plane the region from PU.QS18.L to PU.QS18.R has been used for the analysis. The fits have not been extended further out into the regular arc cells to avoid possible problems due to coupling from the sextupoles. The fit has the same form than for the horizontal plane, but with the vertical optical functions. The vertical betatron function at the IP is $\beta_y^* = 5$ cm for the physics optics. In the region of interest for the fit β_y varies between 10 and 350 m at the orbit monitors. Unfortunately the accuracy of the pickups is not good enough to extract the collision offset with an accuracy much better than about $1-2$ μm compared to beam sizes of about 6 μm. In addition the effect of the small vernier separator bump used to tune to collision offset would have to be taken into account. But the fits give accurate results on crossing angles which are of interest for the alignment of the detectors. An example of a fit is shown in Figure 2. The systematic error on the vertical crossing angle is estimated to be around ± 20 μrad.

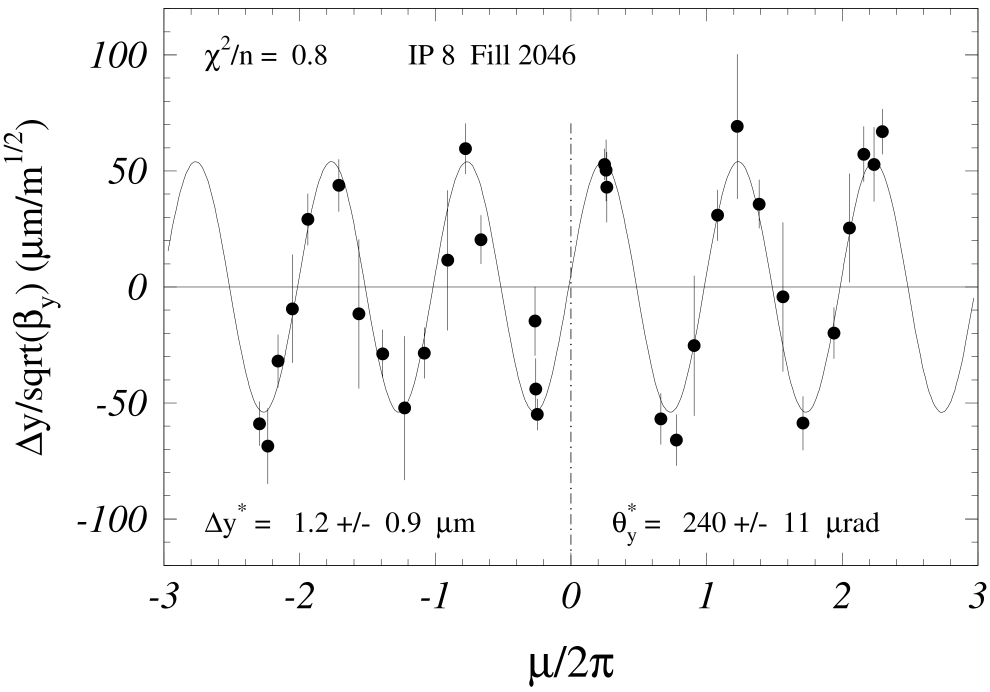

Figure 2: Example of the fit of a measured vertical e^+e^- difference orbit between PU.QS18.L8 and PU.QS18.R8. The difference orbit normalized by the square root of β_y is shown as a function of the vertical phase advance μ around IP8. The IP corresponds to $\mu = 0$. The fitted oscillation is superposed on the data points.

4.3 Results on Horizontal Collision Offsets

The analysis of the horizontal collision offsets reveals large offsets during parts of the 1993 energy scan. The maximum offsets of 150 μm are comparable in size to σ_x^*. The evolution and distributions of the collision offsets Δx^* are shown in Figures 3 to 6. The average offset reached 40 μm in 1993 in IP2 and IP6 which corresponds to $\approx \sigma_x^*/6$. In 1994 the collision offsets have been corrected at the beginning of the run [11]. The reloading of identical settings for each fill guaranteed the stability of the collision offsets. Table 1 gives a summary of the measured offsets.

4.4 Results on Crossing Angles at the Interaction Points

The evolution of the horizontal crossing angle θ_x^* is shown in Figures 7 and 8. These angles have been small and stable in both years. Only the crossing angle in IP2 reached a value of about 50 μrad during a large fraction of 1993. In the LEP coordinate system used throughout

	IP2	IP4	IP6	IP8	Average
1993 : Δx^* [μm]	43 $\pm$ 1	-22 $\pm$ 1	42 $\pm$ 1	11 $\pm$ 1	19 $\pm$ 8
1994 : Δx^* [μm]	18 $\pm$ 1	-19 $\pm$ 1	13 $\pm$ 1	11 $\pm$ 1	6 $\pm$ 8

Table 1: Summary of average horizontal collision offsets in 1993 and 1994. For the LEP average the total error including the systematic error is given. For the individual IPs the systematic error is $\pm$15 μm.

this report, a positive horizontal crossing angle angle corresponds to a net momentum of the e^+e^- system pointing out of the ring (in the direction of increasing radius).

The situation is different for the vertical crossing angles shown in Figures 9 and 10. In 1994 LEP has been running with large crossing angles of about 250 μrad in all experiments. In the LEP coordinates system a positive crossing angle corresponds to a vertical momentum of the e^+e^- system. The sign of the crossing angle changed after a technical stop in June 1994. The origin of the crossing angles might be coupling of the horizontal Pretzel into the vertical plane or an unclosed vertical separation bump in IPs 1,3,5 or 7. This crossing angle did not harm the LEP performance since the beam-beam tune shifts reached values of 0.04 in normal operation. For this reason no attempt was made to correct this situation. The cause for the sign change after the June stop is not understood. The sign and the evolution of the crossing angle have been confirmed by the ALEPH, OPAL and DELPHI experiments where it explained certain problems with the alignment of the detectors. A characteristic feature of the crossing angles is the high degree of correlation between the four IPs which is explained by the fact that the vertical betatron phase advance between two IPs is very close to $19 \cdot 2\pi$.

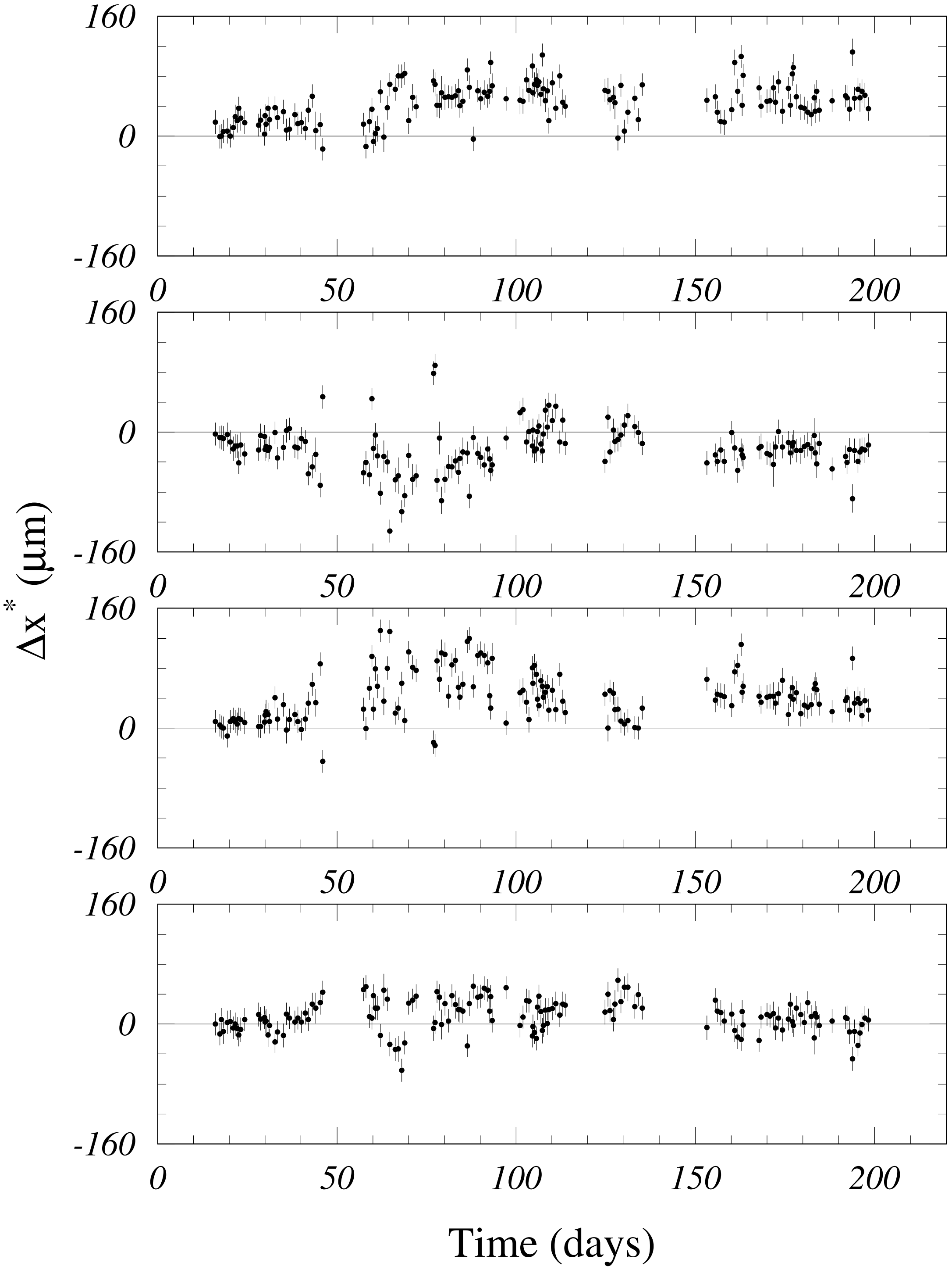

Figure 3: Evolution of the horizontal collision offset Δx^* in 1993. Each point corresponds to the average over one fill. The time scale start on May 1st 1993. The figures correspond to IPs 2 (top) to 8 (bottom). Large fluctuations can be seen in the middle part of the year where collision offsets as large as 150 μm can be observed.

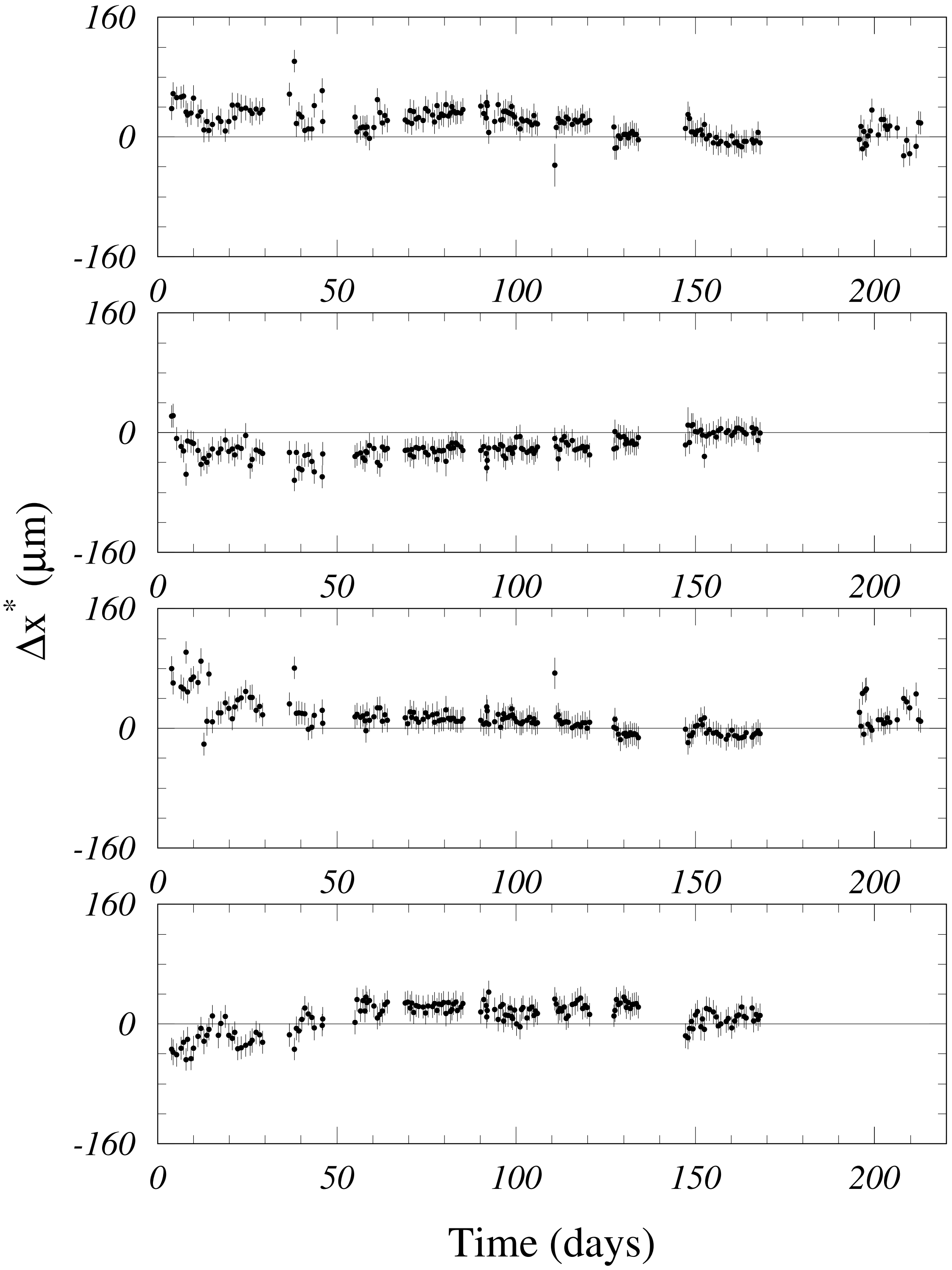

Figure 4: Evolution of the horizontal collision offset Δx^* in 1994. Each point corresponds to the average over one fill. The time scale start on May 1^{st} 1994. The figures correspond to IPs 2 (top) to 8 (bottom). Contrary to 1993 all offsets are close to zero because they have been adjusted at the beginning of the run. No data is available for IPs 4 and 8 in the last period of 1994 during the bunch train test period.

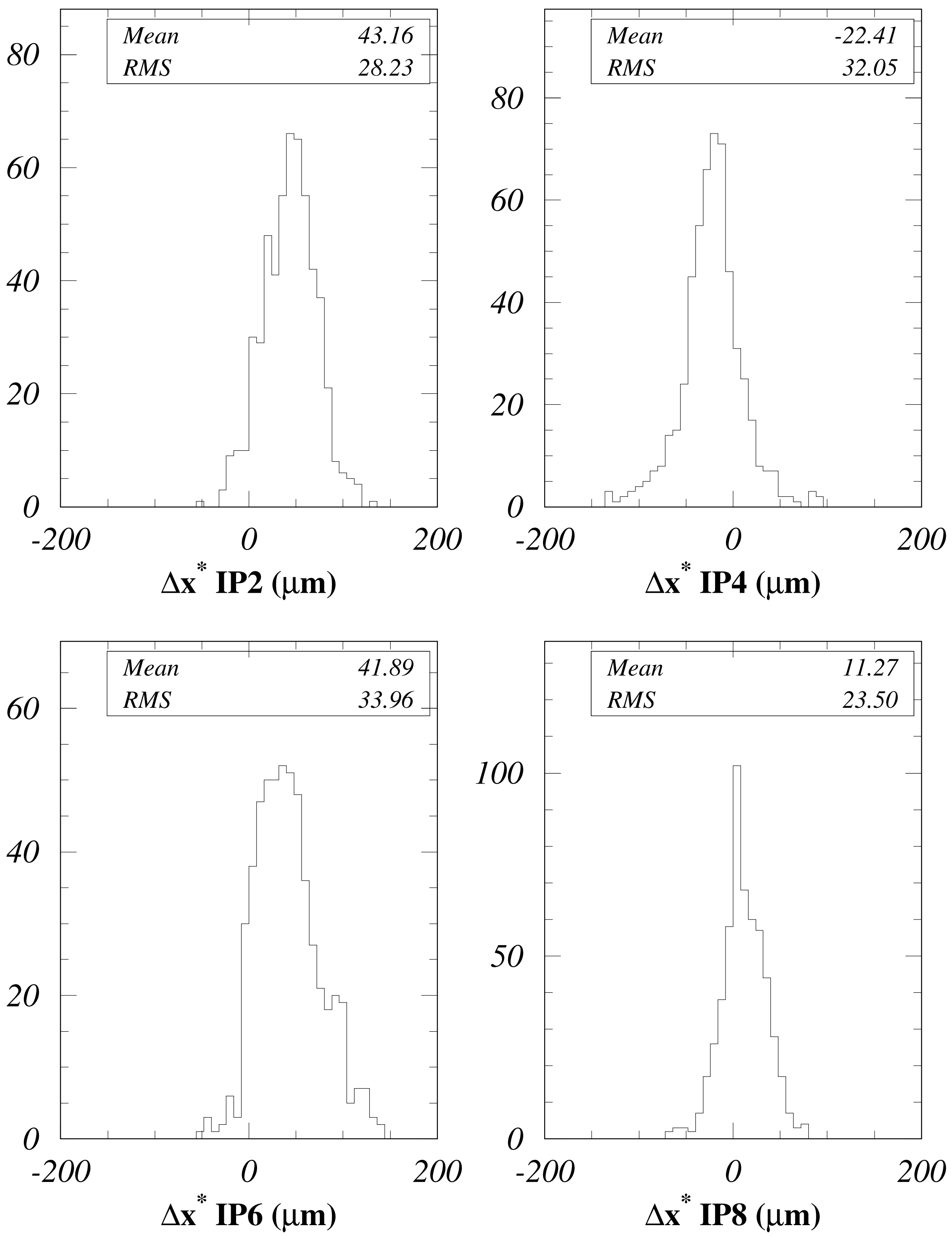

Figure 5: Distribution of the horizontal collision offsets Δx^* in 1993 for the 4 LEP experiments.

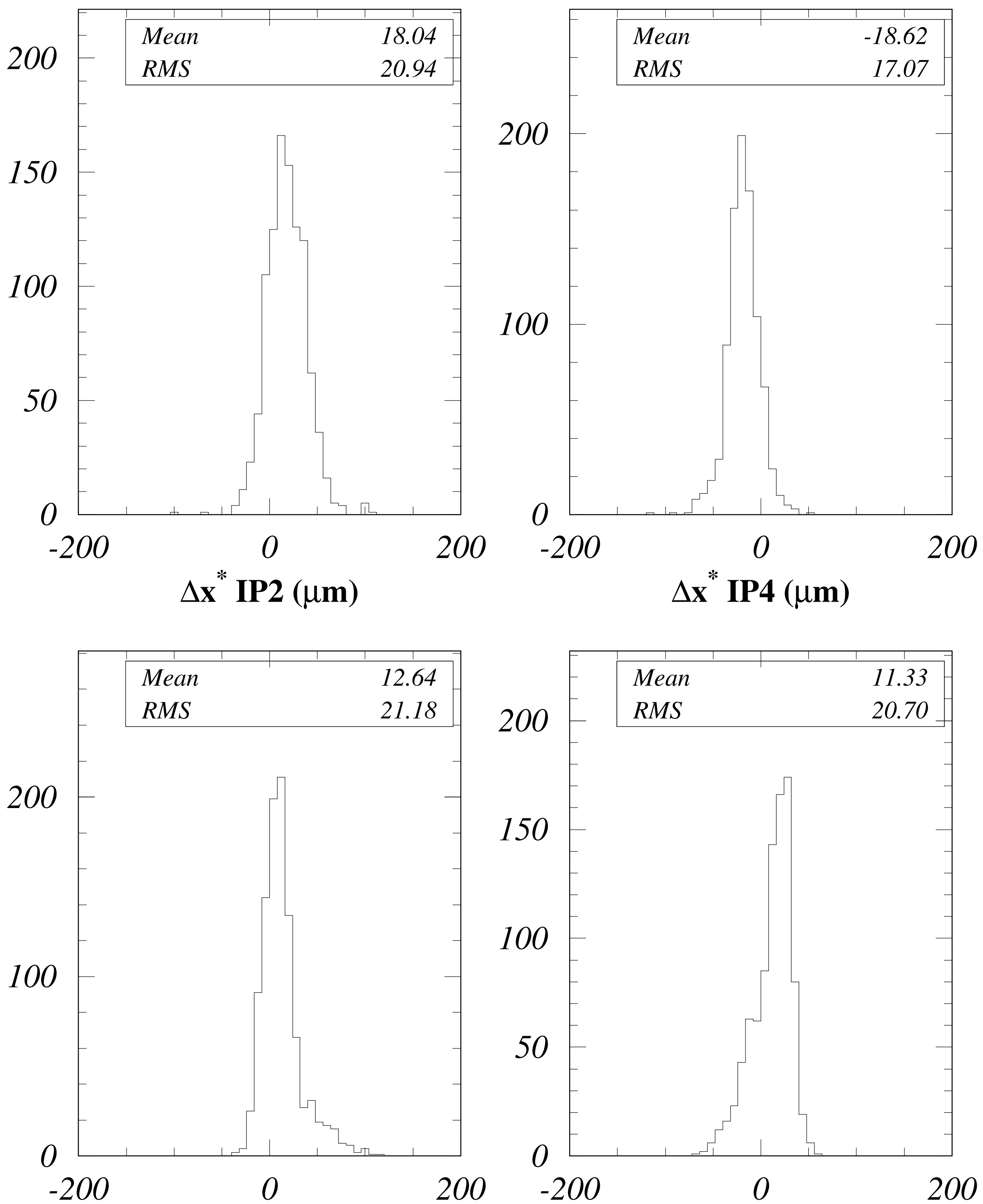

Figure 6: Distribution of the horizontal collision offsets Δx^* in 1994 for the 4 LEP experiments.

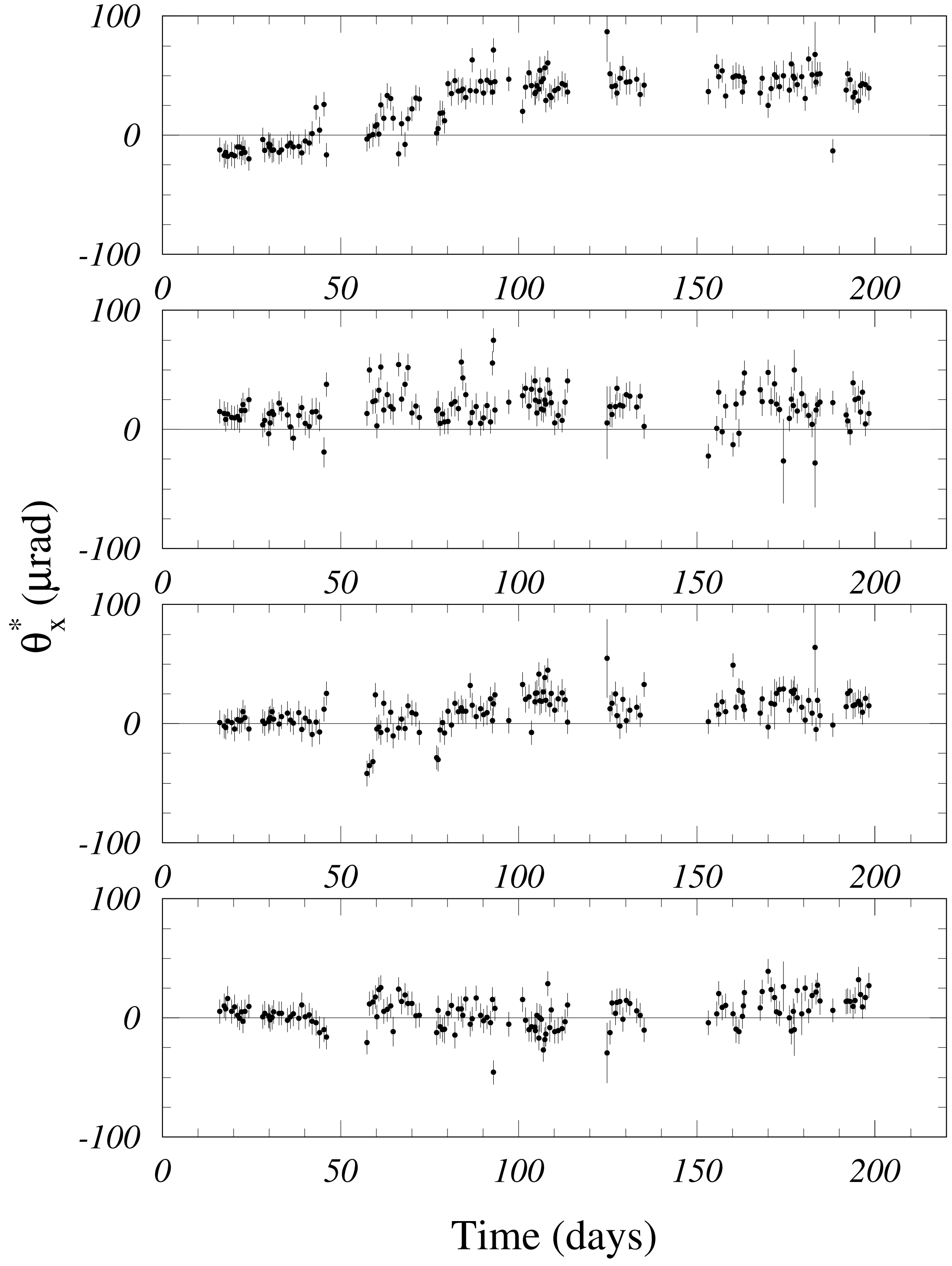

Figure 7: Evolution of the horizontal crossing angles θ_x^* in 1993. Each point corresponds to the average over one fill. The time scale start on May 1^{st} 1993. The figures correspond to IPs 2 (top) to 8 (bottom).

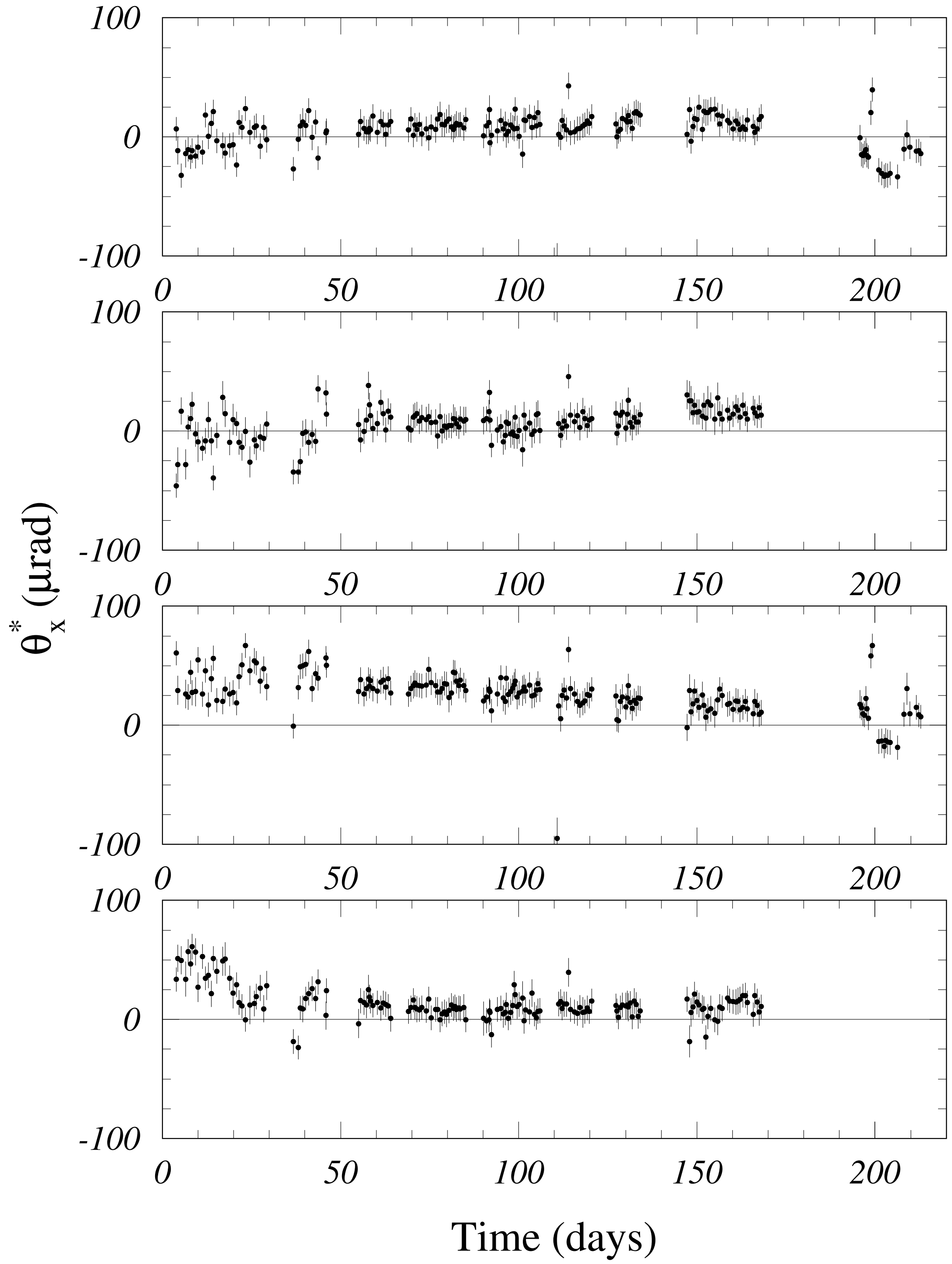

Figure 8: Evolution of the horizontal crossing angles θ_x^* in 1994. Each point corresponds to the average over one fill. The time scale start on May 1^{st} 1994. The figures correspond to IPs 2 (top) to 8 (bottom).

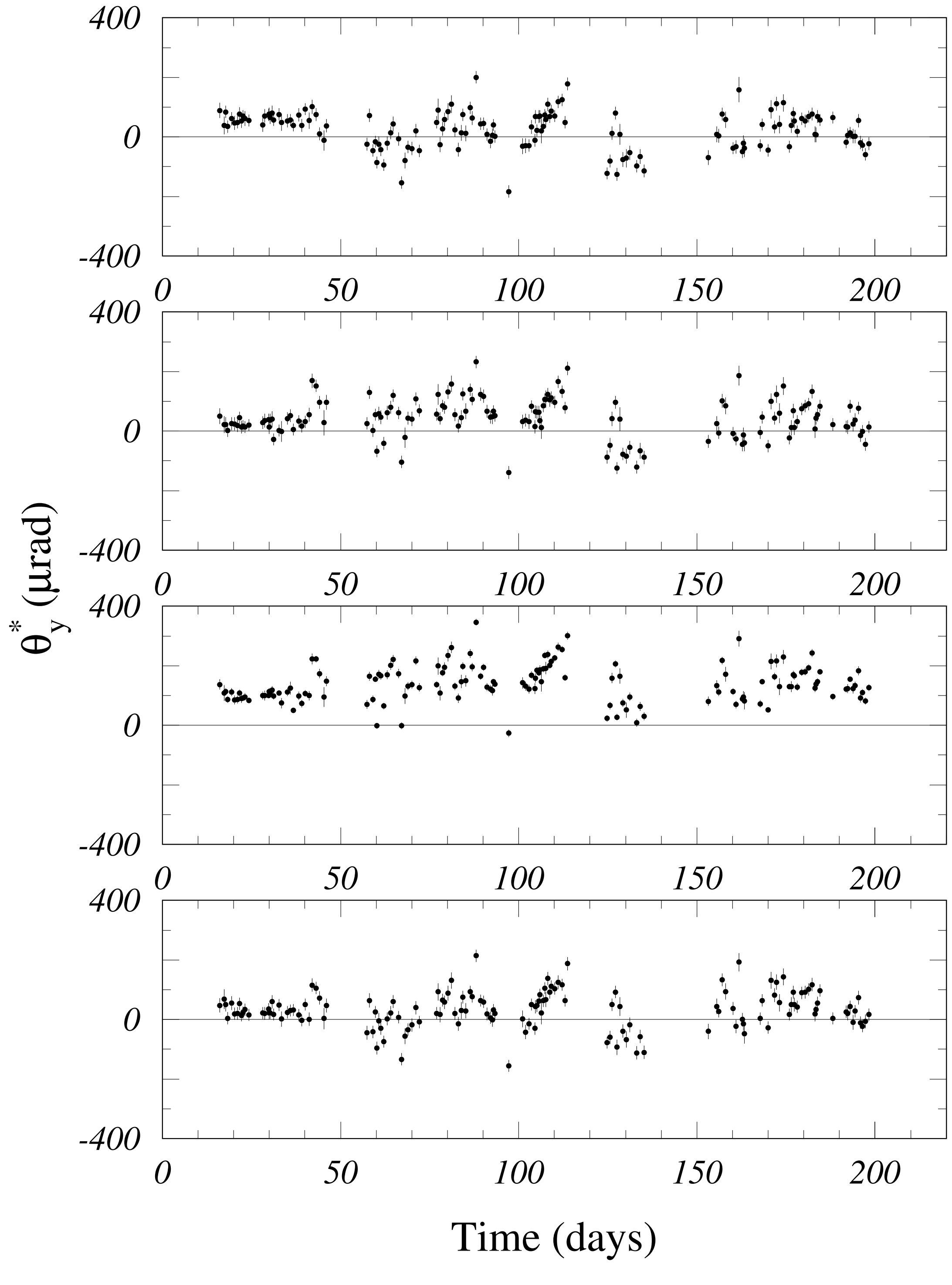

Figure 9: Evolution of the vertical crossing angles θ_y^* in 1993. Each point corresponds to the average over one fill. The time scale start on May 1^{st} 1993. The figures correspond to IPs 2 (top) to 8 (bottom).

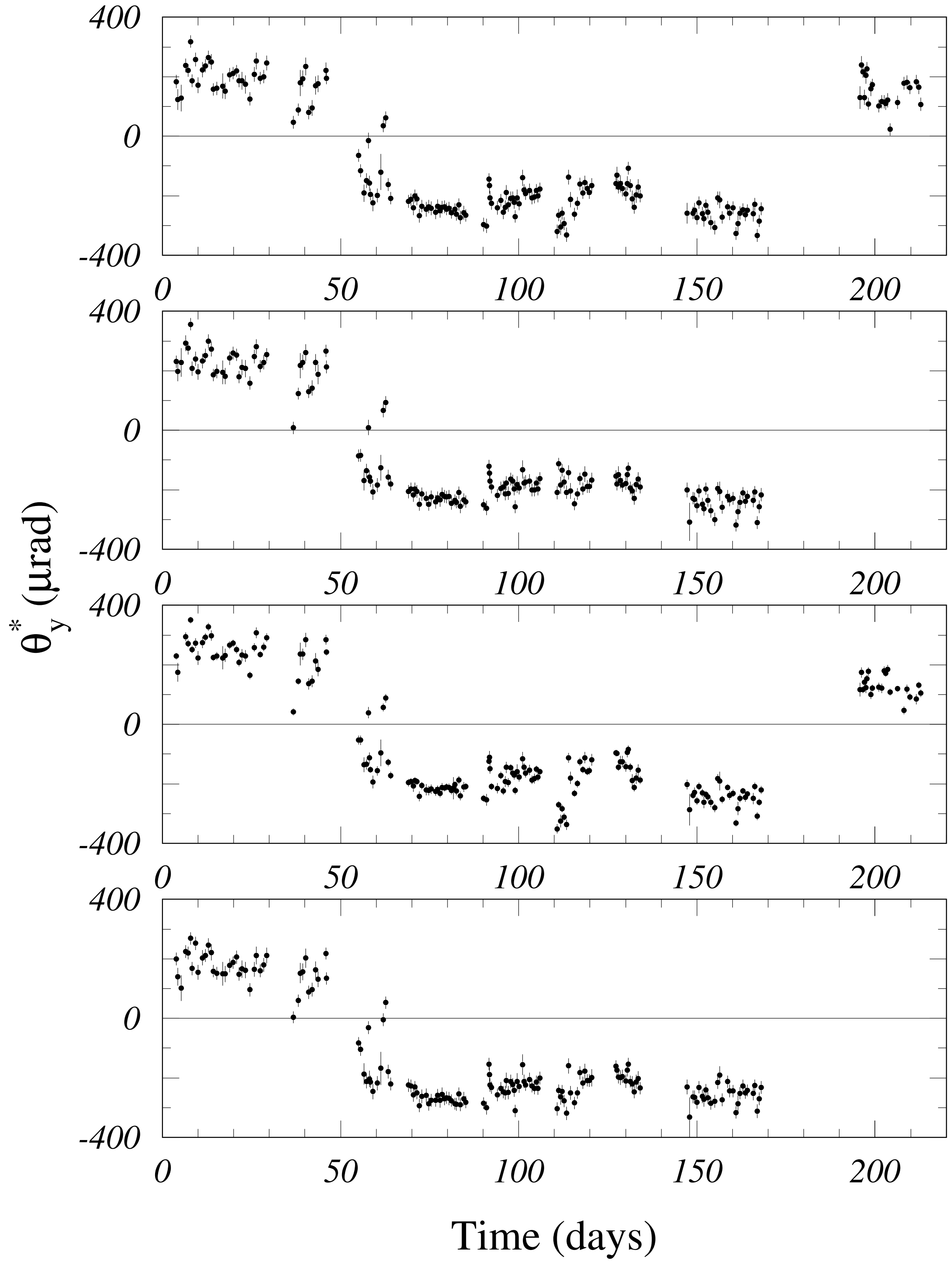

Figure 10: Evolution of the vertical crossing angles θ_y^* in 1994. Each point corresponds to the average over one fill. The time scale start on May 1^{st} 1994. The figures correspond to IPs 2 (top) to 8 (bottom). LEP has been running with vertical crossing angles throughout the year. There is a change in sign of the crossing angle after the June technical stop. For the last period (after day 190) no reliable data is available for IPs 4 and 8 where the vertical electrostatic bunch train bumps were used.

5 Periodic Dispersion

As has been pointed out in section 2, the correlation between energy and transverse position introduced by a difference in dispersion between the two beams is at the origin of the monochromator effect.

The dispersion $D(s)$ in a storage ring of circumference L is a periodic function which depends on the deflections in all elements of the lattice along the closed orbit :

$$D(s) = \frac{\sqrt{\beta(s)}}{2\sin(\pi Q)} \oint_{s}^{s+L} \frac{\sqrt{\beta(t)}}{\rho(s)} \cos(\mu(s) - \mu(t) - \pi Q)dt \tag{11}$$

ρ is the local radius of curvature of the orbit. While the closed orbit (Equation 6) depends only on deflections encountered on the *ideal orbit*, all deflections of the *closed orbit* must be taken into account in Equation 11 for $D(s)$. In general it is complicated to extrapolate the dispersion measured at pickups to another point of the machine because all the details of the deflections have to be known for the orbit under consideration. The situation is simpler for the difference dispersion $\Delta D(s)$ between the e^+ and e^- beams. In that case many magnetic elements give (almost) equal contributions to both beams and a large fraction of their effects cancels for the extrapolation of $\Delta D(s)$. From Equation 11 we note that $\Delta D(s)$ receives contributions from the following sources :

- Electrostatic elements give large contributions since $\rho_{e-} = -\rho_{e+}$.
- Differences in energy caused by the energy sawtooth lead to $\rho_{e-} \neq \rho_{e+}$.
- Orbit differences Δu of the two beams lead to $1/\rho_{e-} - 1/\rho_{e+} \sim \Delta u$ in quadrupoles. A quadratic dependence on Δu is obtained in sextupoles.

In a region without sources of dispersion $D(s)$ behaves like a betatron oscillation. In the case of a single source of dispersion Equation 11 leads to :

$$D(s) = \frac{\sqrt{\beta(s)}}{2\sin(\pi Q)} \sqrt{\beta_i}\theta_i \cos(|\mu(s) - \mu_i| - \pi Q) \tag{12}$$

where θ_i is the deflection at source i. This simple behavior can be used to extract the dispersion difference at the IP ΔD^* from a fit of $\Delta D(s)$ through the straight sections around the collision points. In a region free of elements contributing to $\Delta D(s)$, its evolution is described by :

$$\frac{\Delta D(s)}{\sqrt{\beta(s)}} = A\cos(\mu(s)) + B\sin(\mu(s)) \tag{13}$$

which is identical to the behavior of the difference orbits analyzed in the previous section. The dispersion at the IP is then given by :

$$\Delta D^* = \sqrt{\beta^*} A \tag{14}$$

provided the phase is defined such that $\mu = 0$ at the IP.

6 Analysis of the Difference Dispersion

The dispersion is measured periodically in LEP to understand or control the machine performance. The number of measurements taken with the physics optics at 45 GeV that have been

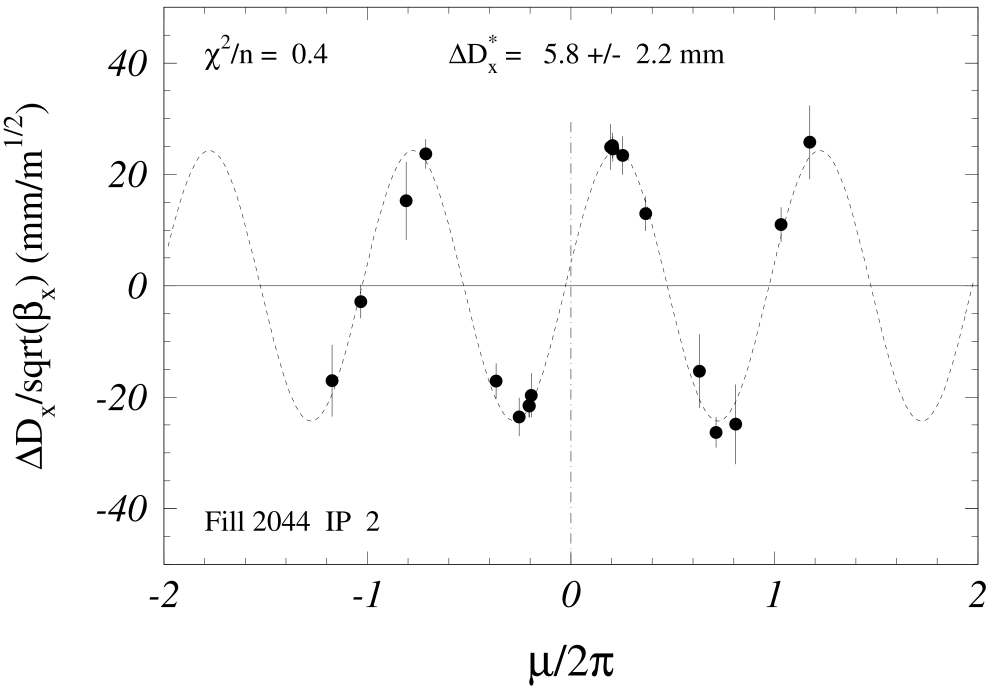

Figure 11: Example of the fit of the measured horizontal e^+e^- difference dispersion between PU.QS10.L2 and PU.QS10.R2. The difference dispersion is normalized by the square root of β_x and shown as a function of the horizontal phase advance μ around the IP. The IP corresponds to $\mu = 0$. The fitted oscillation is superposed on the data points.

recovered is 17 for 1993 and 37 for 1994. To measure the dispersion two orbits are acquired with different settings of the RF frequency. From the known difference in energy and the measured orbit position change at the beam orbit monitors, the dispersion is extracted using Equation 1. The typical change in RF frequency was 100 Hz which corresponds to a relative energy variation $\delta E/E = 1.6 \cdot 10^{-3}$. The data samples are small, but they should still be representative of the typical situation since it is expected that most of the difference dispersion is due to imperfections and electrostatic elements which do not evolve much with time.

6.1 Fit of the Horizontal Difference Dispersion

The horizontal difference dispersion is analyzed in the same fashion than the difference orbits using again the pickup range from PU.QS10.L to PU.QS10.R. No particular attention has to be paid to the fact that the beams are colliding or are vertically separated at the IP since the vertical separators do not affect ΔD_x^* in a significant way through coupling. A measurement error of 60 μm on the difference between the two orbits has been used in the fits. An example is shown in Figure 11. The systematic error on ΔD_x^* is estimated to be about ± 3 mm. This systematic error is largely uncorrelated between the IPs because it is dominated by beam orbit monitor errors.

6.2 Fit of the Vertical Difference Dispersion

The analysis of the vertical difference dispersion is more complicated because the electrostatic bumps used to separate the beams at IPs 2, 4, 6 and 8 can perturb the smooth evolution of ΔD_y

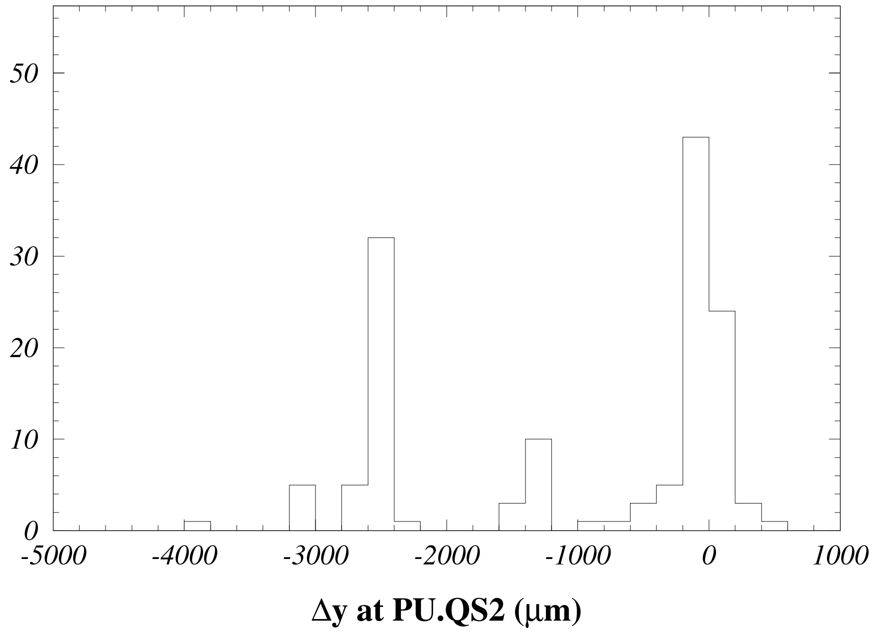

Figure 12: Distribution of the average vertical separation in PU.QS2.L and PU.QS2.R for the 1994 dispersion data sample and for all IPs. Only measurements with an absolute separation of less than 500 μm are used for the analysis of the vertical dispersion. The nominal separation is about 2500 μm at the pickups PU.QS2.

through the straight sections since they are sources of difference dispersion. The effect of these bumps can in principle be calculated with the MAD program, but to be independent of any model, dispersion measurements performed with colliding beams or with beams that have only a small separation at the IP have been selected in the sample. The data is filtered with one of the two orbits that correspond to each dispersion measurement. The electrostatic separator bumps separate the beams by a large amount in the pickups PU.QS2.L and PU.QS2.R. The average vertical position difference of the beams in these two monitors is used to identify measurements performed with large beam separations. The distribution of the vertical separation in PU.QS2 is shown in Figure 12 for the 1994 data sample. Only measurements with a separation of the two orbits of less than 20% of the nominal amplitude are used for the analysis. The residual dispersion that is generated with such small separations is negligible. This cut does not guarantee that the beams were actually colliding during the measurement. After applying the cut we are left with 13 measurements for 1993 and 22 measurements for 1994.

Figure 13 shows two examples of fits of ΔD_y around the IP. Each fit has been performed independently for the left (L) and right (R) side. The extrapolations to the IP disagree significantly for the two sides. This points towards a discontinuity of the dispersion between PU.QS0.L and PU.QS0.R. Since a difference in dispersion generated by the beam-beam interaction would only lead to a discontinuity of the slope of ΔD_y at the IP, the source of the discontinuity must be the superconducting QS0 quadrupoles located between the last pickup and the IP. As has been pointed out previously, the QS0 quadrupoles create vertical difference dispersion when a vertical crossing angle at the IP leads to a separation of the beams in the QS0. The systematic shift between the values of ΔD_y^* extracted from a fit of the left and right

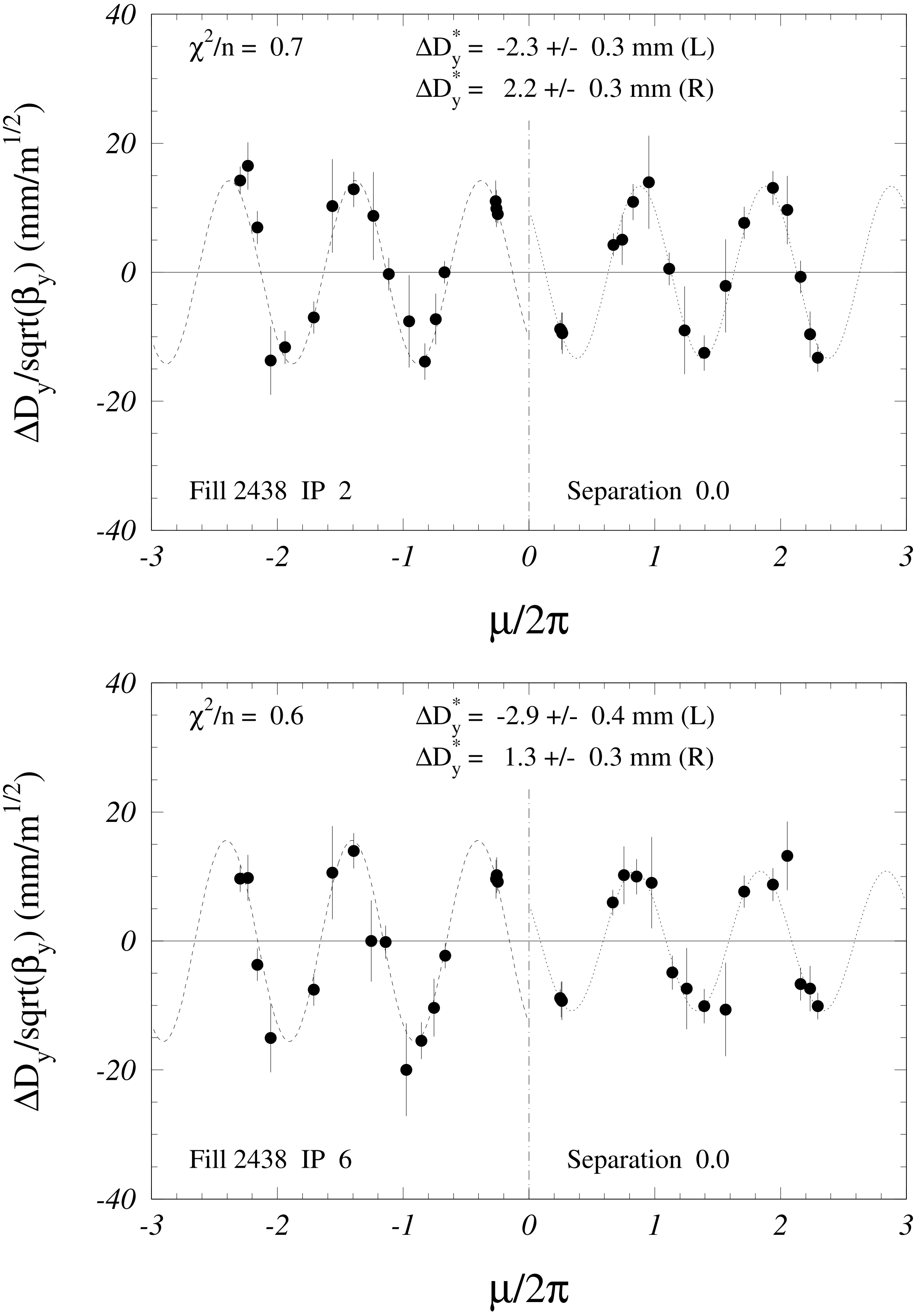

Figure 13: Examples of the fit of the measured vertical e^+e^- difference dispersion ΔD_y between PU.QS18.L and PU.QS18.R. ΔD_y is normalized by the square root of β_y and shown as a function of the vertical phase advance μ around the IP. The IP corresponds to $\mu = 0$. The fits are performed independently for the left (L) and right (R) side and exhibit significant discontinuities at the IP. The superconducting quadrupoles installed between the last pickup and the IP are the source of the discontinuity.

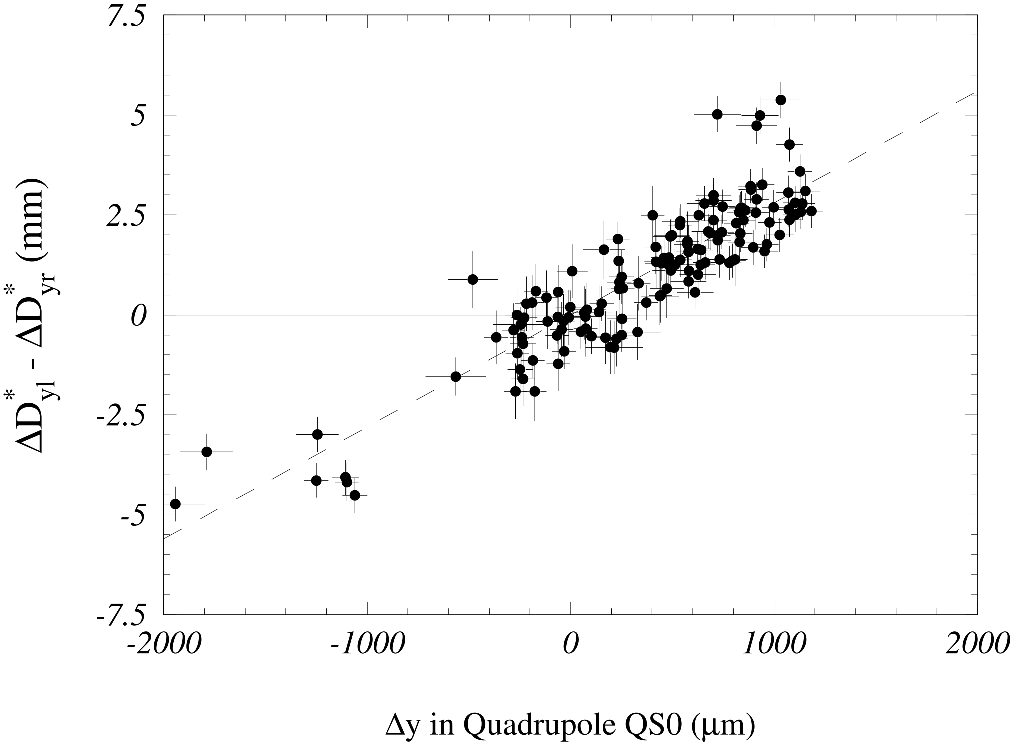

Figure 14: Correlation between the difference of the extrapolated e^+e^- difference dispersions for the left (ΔD^*_{yl}) and right (ΔD^*_{yr}) side of the IP and the separation of the beams in the QS0 quadrupole. The dotted line shows the expected correlation if the superconducting QS0 quadrupoles are the cause of the left-right difference. This figure contains the 1993 and 1994 data samples.

side of the IP can be estimated to be :

$$\Delta D^*_{yl} - \Delta D^*_{yr} = 2\sqrt{\beta_{QS0}\,\beta^*}\,KL\,\Delta y = 2\,\beta_{QS0}\,\beta^*\,KL\,\theta^*_y = 2.8\cdot\Delta y \qquad (15)$$

Δy is the separation of the two beams in the QS0 quadrupole and $KL = 0.32$ (m^{-1}) is the QS0 quadrupole focusing strength ($\beta_{QS0} = 380$ m). To test this model, a difference orbit corresponding to each dispersion measurement has been analyzed using the orbit fit described previously. The vertical separation of the beams in the QS0 has been extracted from this fit. The separation is correlated with $\Delta D^*_{yl} - \Delta D^*_{yr}$ in Figure 14. The good correlation shows that the model accounts for most of the discontinuity around the IPs. Obviously other quadrupoles can also degrade the quality of the correlation but their individual contributions are at least a factor 8 smaller because of their weaker gradients and smaller betatron functions. The good quality of the fits on both sides of the IPs is another indication that the perturbation due to separation of the beams in other quadrupoles is small. The separation Δy in the QS0 can be used to correct the fitted values of ΔD^*_y. Because of the symmetry of the perturbation of the two QS0 quadrupoles the dispersion at the IP is simply obtained by averaging the fit results from the left and the right side :

$$\Delta D^*_y = \frac{1}{2}\left(\Delta D^*_{yl} + \Delta D^*_{yr}\right) \qquad (16)$$

From the residual difference between ΔD^*_{yl} and ΔD^*_{yr} after correction for the QS0 effect, a systematic error of ± 0.2 mm, uncorrelated between the IPs, is assigned to ΔD^*_y. An additional error of ± 0.2 mm is assigned to the perturbation of the fit due to separation of the beams in other quadrupoles than the QS0. This contribution is estimated using different combinations of monitors for the fits. Since the crossing angles show important correlations between the IPs, this contribution to the systematic error is correlated between IPs. This leads to a total systematic error on ΔD_y^* of ± 0.3 mm for each IP. Taking into account the quoted correlation the systematic error on the LEP average over all IPs is ± 0.2 mm.

6.3 Results on Difference Dispersions at the Interaction Points

The results of all fits for 1993 and 1994 are shown in Figures 15 to 18. For the individual IPs the average horizontal dispersion was smaller than 3 mm and its RMS spread was typically 5 mm. No structure is observed as a function of time. The distributions of ΔD_y^* shown in Figures 17 and 18 give a mean difference dispersion of 0.4 mm for 1993 and 0.6 mm for 1994. The RMS spread is 0.5 to 1.0 mm and there is no time dependence. The residual vertical difference dispersion seems to be correlated between the four IPs. Table 2 summarizes the results on dispersions at the IPs. The average of ΔD_x^* over all IPs is compatible with zero and a small deviation from zero is measured for ΔD_y^*. For the bunch train scheme the expected vertical difference dispersions of 2 to 4 mm are much larger than the values measured here for the Pretzel scheme.

	IP2	IP4	IP6	IP8	Average
1993 run :					
ΔD_x^* [mm]	1.6 ± 1.3	0.8 ± 1.4	0.7 ± 1.1	-0.9 ± 2.0	$0.6 \pm 0.7 \pm 1.5$(sys)
ΔD_y^* [mm]	0.4 ± 0.1	0.4 ± 0.2	0.2 ± 0.2	0.6 ± 0.2	$0.4 \pm 0.1 \pm 0.2$(sys)
1994 run :					
ΔD_x^* [mm]	0.9 ± 0.7	-0.4 ± 0.7	0.6 ± 0.7	-2.9 ± 0.6	$-0.5 \pm 0.4 \pm 1.5$(sys)
ΔD_y^* [mm]	0.6 ± 0.2	0.5 ± 0.2	0.6 ± 0.2	0.7 ± 0.3	$0.6 \pm 0.1 \pm 0.2$(sys)

Table 2: Summary of average difference dispersions for all IPs in 1993 and 1994. The systematic error is only shown for the LEP average. For the individual IPs the systematic errors are 3 mm on ΔD_x^* and 0.3 mm on ΔD_y^*.

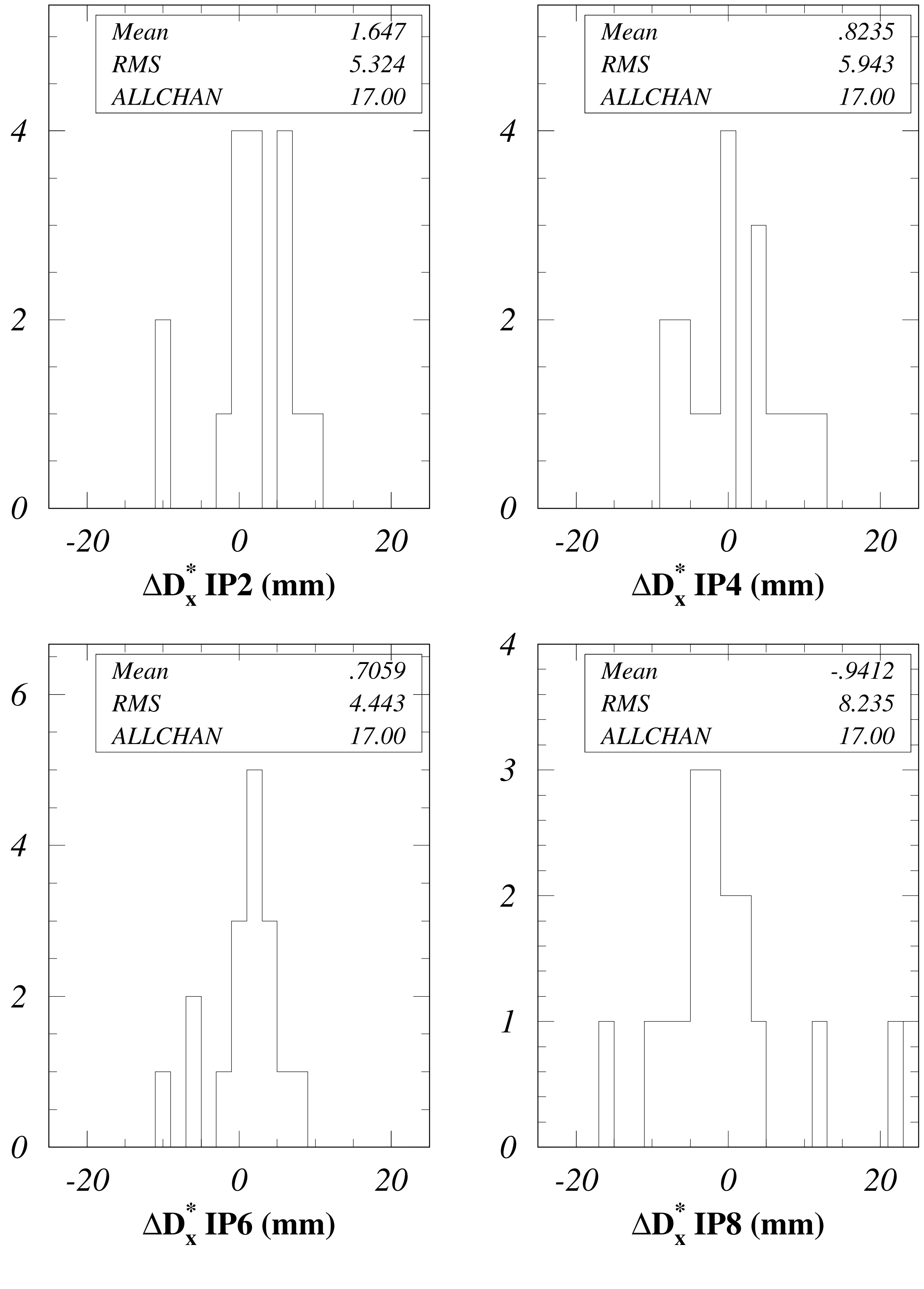

Figure 15: Distribution of the horizontal difference dispersion at the IPs in 1993.

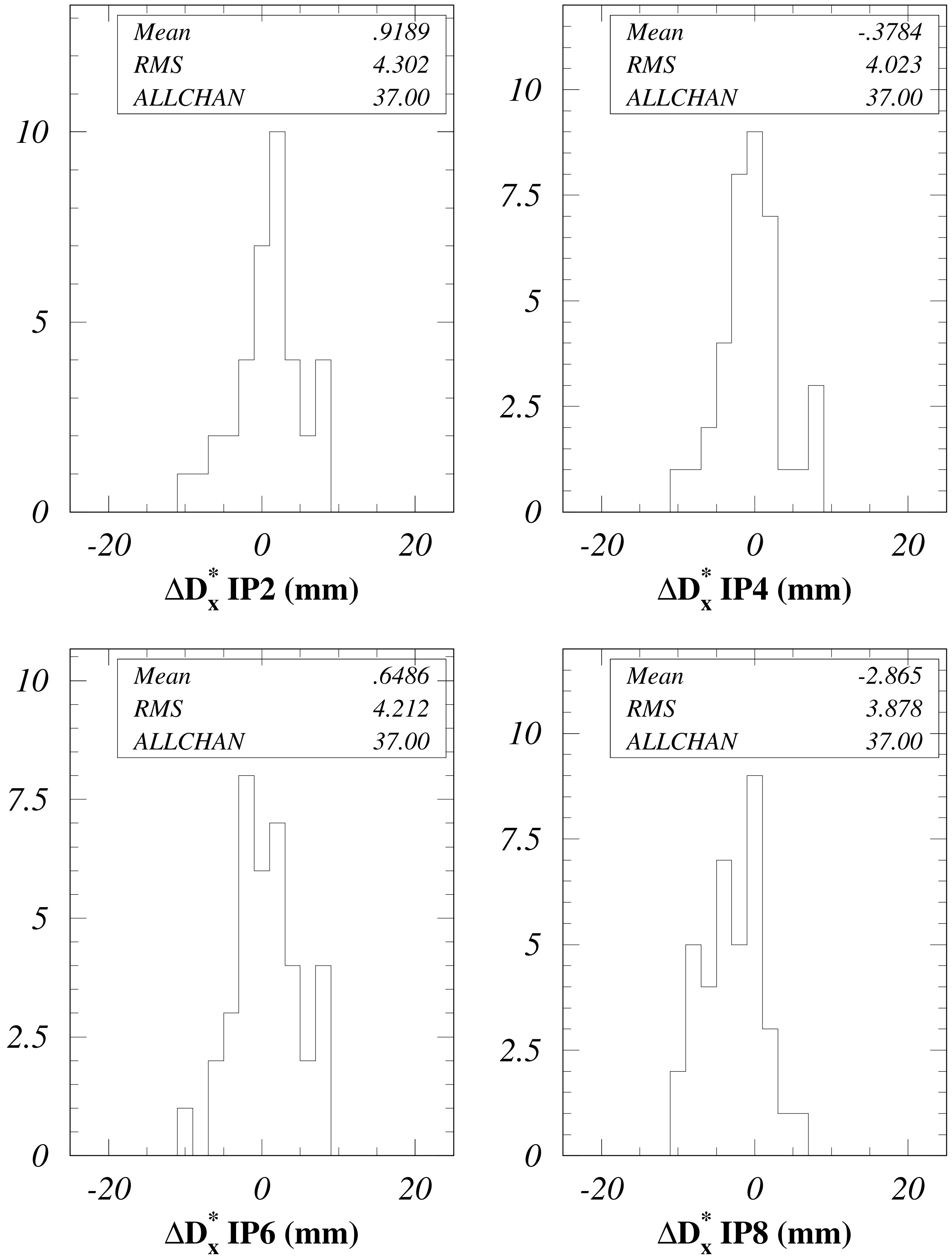

Figure 16: Distribution of the horizontal difference dispersion at the IPs in 1994.

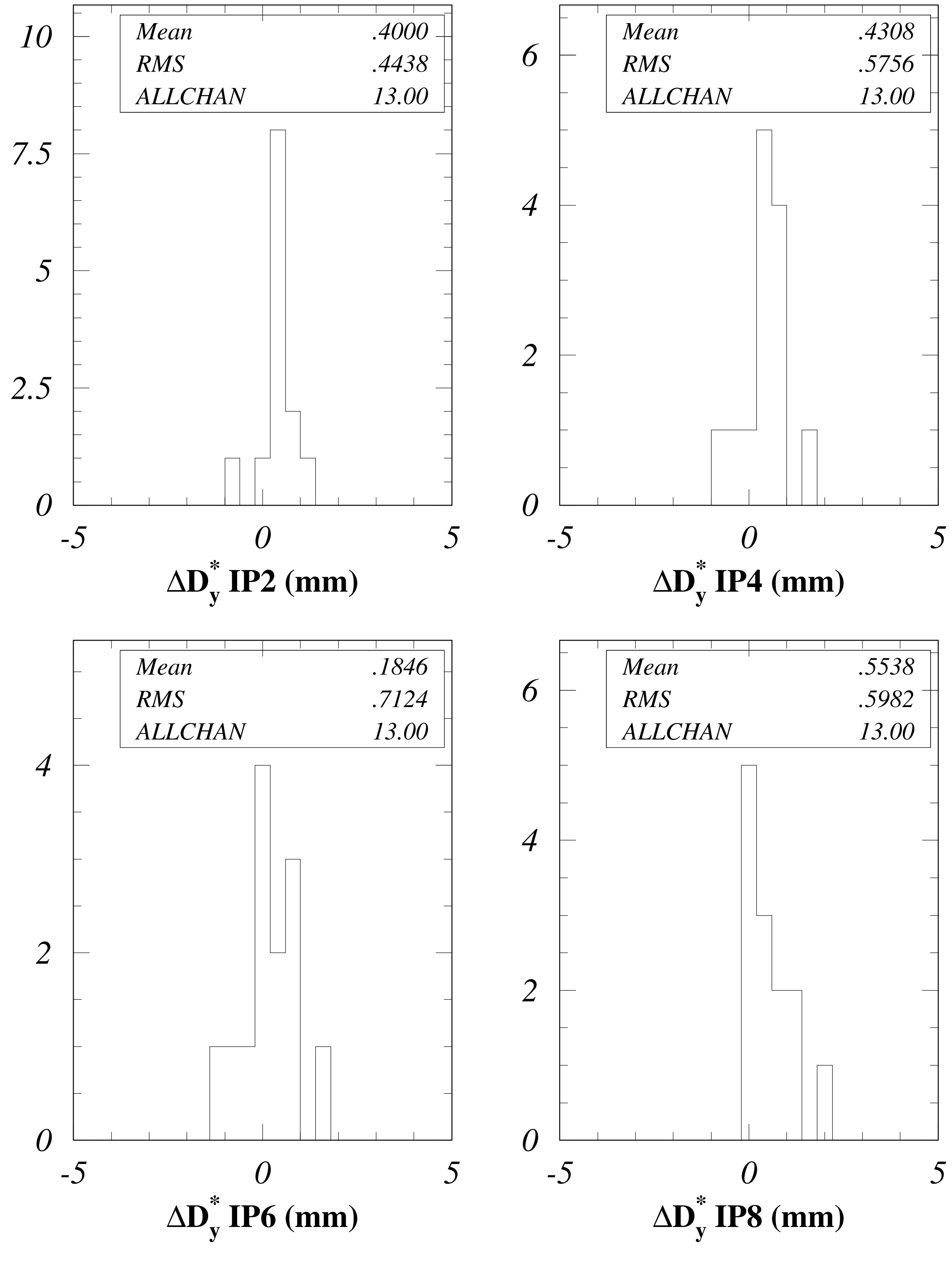

Figure 17: Distribution of the vertical difference dispersion at the IPs in 1993.

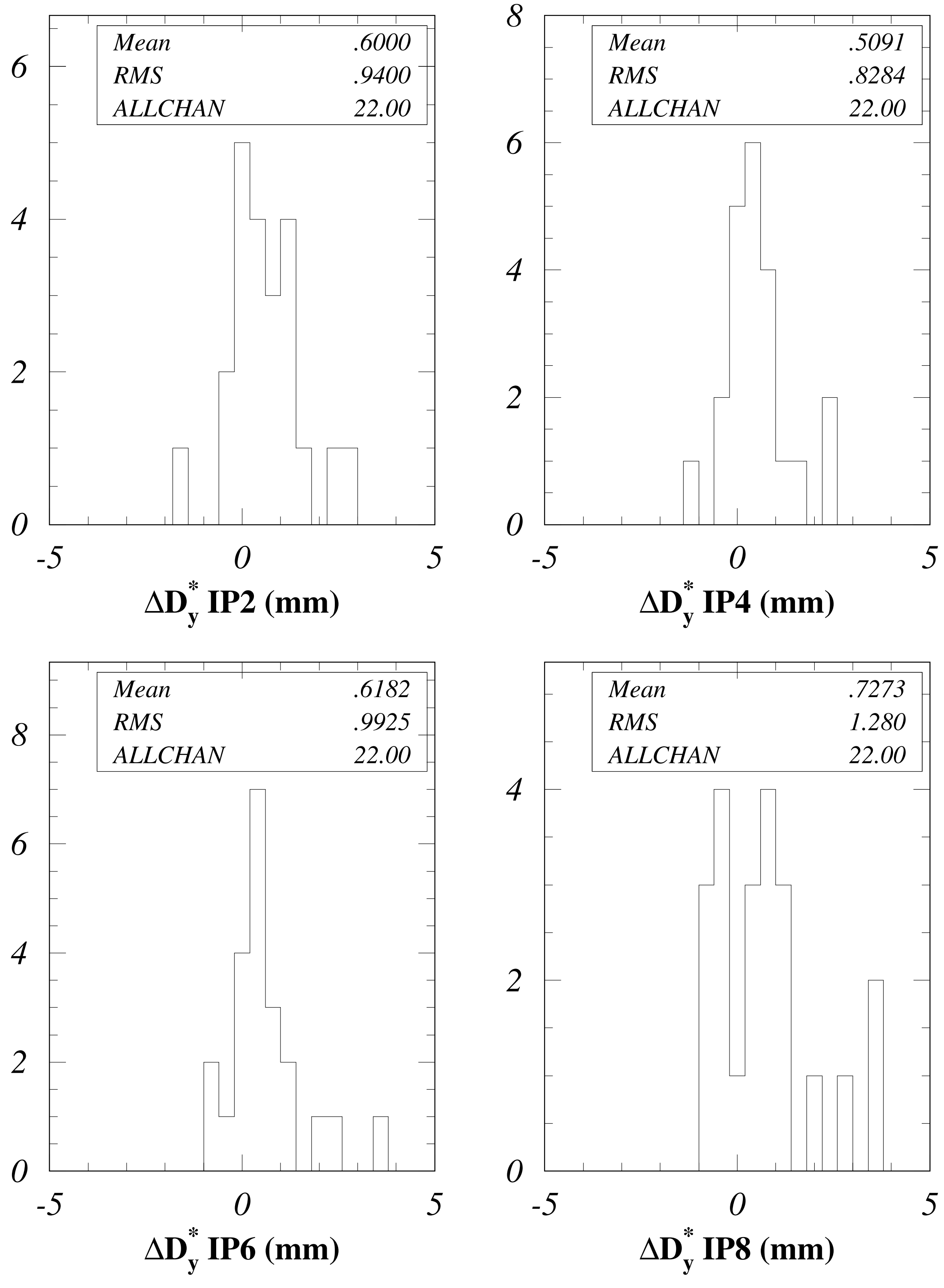

Figure 18: Distribution of the vertical difference dispersion at the IPs in 1994. There is a correlated shift between all IPs.

7 Systematic Effects on the Centre-of-Mass Energy

We can use the measured parameters to evaluate the impact of the monochromator effect on the CM energy distributions taking roughly into account the correlations of energy spread and beam sizes. In the course of a fill the relative energy spread σ_E/E varies from $1.1 \cdot 10^{-3}$ down to $0.7 \cdot 10^{-3}$ as the field of the emittance wigglers is slowly ramped down. In parallel the horizontal beam emittance ε_x evolves from about 40 nm down to 20 nm [12] and the horizontal beam size at the IP from about 280 to 200 μm ($\beta_x^* = 2$ m). In 1993 the horizontal beam sizes were 12% larger because of a larger β_x^* of 2.5 m. The vertical beam emittance is very small and therefore difficult to measure accurately. For this reason the vertical beam size at the IP σ_{by}^* is extracted from the observed luminosities [12, 13]. For a good performance 1994 Pretzel fill with initial luminosities of $1.6 \cdot 10^{31}$ cm^{-2} s^{-1}, σ_{by}^* evolved from about 5 to 3 μm during the coast. Since in 1993 the typical luminosities at the start of fill were lower and reached only typically $1.2 \cdot 10^{31}$ cm^{-2} s^{-1}, the vertical beam sizes at the IPs were roughly 20% larger than in 1994.

Table 3 shows the CM energy shifts that are expected for certain combinations of the parameters entering Equation 2 for ΔE_{CM}. For an average ΔD_x^* of 1 mm and a collision offset of 20 μm the CM energy shift is less than 10 keV. Even with an average ΔD_x^* of 10 mm the observed average collision offset would therefore not lead to a significant uncertainty on the CM energy. For the vertical plane the average collision offset could not be measured. But it is safe to assume that averaged over one year, the collision offset has not exceeded ~ 1 μm. The measured average difference dispersions lead to an uncertainty on the CM energy of about 0.4 MeV for 1993 and 0.7 MeV for 1994. These CM energy errors are probably correlated between the 1993 scan points. The correction to the CM energy spread $\sigma_{E_{CM}}$ with respect to the situation where the beam energy spread of the two beam adds up incoherently is negligible for both runs.

Plane	σ_{bu}^* [μm]	σ_E/E [10^{-3}]	Δu^* [μm]	ΔD_u^* [mm]	$\lvert\Delta E_{CM}\rvert$ [MeV]	$\sigma_{E_{CM}}/\sqrt{2}\sigma_E$
Horizontal	280	1.1	20	1.0	<0.01	1.000
	200	0.7	20	1.0	<0.01	1.000
Vertical (1993)	6	1.1	1	0.4	0.3	0.999
	3.5	0.7	1	0.4	0.4	0.999
Vertical (1994)	5	1.1	1	0.6	0.7	0.998
	3	0.7	1	0.6	0.7	0.998

Table 3: CM energy shifts ΔE_{CM} and correction to the CM energy spread $\sigma_{E_{CM}}$ for different combinations of beam parameters. For the vertical plane the two sets of numbers correspond to the situations in 1993 and 1994. For each set of values the first (second) line corresponds to beam sizes at the beginning (end) of a fill. Fluctuations of 10 to 20% are possible from fill to fill.

8 Conclusions

The difference dispersion and collisions offsets at the IPs have been extracted for the 1993 and 1994 Pretzel runs of LEP from orbits and dispersion measurements. Although large horizontal collision offset have been present in a fraction of the 1993 energy scan, the average CM energy shift due to the monochromator effect in the horizontal plane can be safely neglected. The accuracy of the orbit measurements is not high enough to extract the vertical collision offsets so that the CM energy shifts can only be estimated for the vertical plane assuming that the average collision offset has not exceeded 1 μm. From the measured difference dispersion we obtain a systematic error from CM energy shifts of 0.4 MeV for the 1993 run and of 0.7 MeV for the 1994 run. This error does not modify significantly the result of the 1993 scan since it is small compared to the ± 1.5 MeV calibration error quoted in [2]. The correction to the CM energy spread does not exceed 0.2% and is still negligible. It is clear from the magnitude of the CM energy uncertainties for Pretzel operation that the monochromator effect must be kept under control in a future energy scan whatever the LEP run scheme (bunch train or Pretzel) if the errors on the Z mass and width should be reduced below the present level.

9 Acknowledgments

I thank R. Schmidt for many useful “brainstorming” discussions.

References

[1] L. Arnaudon et al., "Accurate Determination of the LEP Beam Energy by Resonant Depolarization", Z. Phys. C66 (1995) 45.

[2] R. Assmann et al., "The Energy Calibration of LEP in the 1993 Scan", CERN PPE/95-10 and CERN SL/95-02 (1995). To be published in Z. Phys. C.

[3] C. Bovet et al., “Final Report of the 1994 Bunch Train Study Group”, CERN SL/94-95 (AP).

[4] E. Keil, “Side Effects of Beam-Beam Crossings in Bunch Trains with Head-On Collisions”, CERN SL/94-76 (AP).
E. Keil, “Offsets and Crossing Angles for Trains of Two, Three and Four Bunches”, CERN SL/Note 95-40 (AP).

[5] J.M. Jowett, J. Wenninger, J. Yamartino, “Influence of Dispersion and Collision Offsets on the Centre-of-Mass Energy at LEP”, CERN SL/Note 95-46 (OP).

[6] M. Basseti and J.M. Jowett, “Improving the Energy Resolution of LEP Experiments”, Proc. of the IEEE Particle Accelerator Conference, Washington D.C., March 1987.

[7] H. Wiedemann, “Particle Accelerator Physics”, Springer-Verlag (1994).

[8] H. Grote, C. Iselin, The MAD program V8.10, CERN-SL/90-13 Rev. 3 (AP).

[9] I. Reichel, "Beam position measurements by modulation of quadrupole strengths", CERN SL/Note 95-50 (1995).

[10] P. Castro, Proc. of the Fourth Workshop on LEP performance, CERN SL/94-06 (DI).

[11] The adjustment was performed by J.M. Jowett using difference orbit fits.

[12] H. Burkhardt, private communication.

[13] A. Verdier, private communication.